ACS OMEGA

Open Access

http://pubs.acs.org/journal/acsodf

Article

Degradation Kinetic Studies of BSA@ZIF-8 Nanoparticles with Various Zinc Precursors, Metal-to-Ligand Ratios, and pH Conditions

Jia Gao, Wenhui Chu,* Xuankai Ding, Lingzhi Ding, Qing Guo, and Yongqian Fu*

Cite This: *ACS Omega* 2023, 8, 44601−44610

Read Online

ACCESS | Metrics & More | Article Recommendations | Supporting Information

ABSTRACT: Nanosized zeolitic imidazolate framework particles (ZIF-8 nanoparticles [NPs]) have strong potential as effective carriers for both *in vivo* and *in vitro* protein drug delivery. Synthesis of ZIF-8 and stability of protein encapsulation within ZIF-8 are affected by several factors, notably the metal ion source and molar ratio. To systematically investigate these factors, we investigated such effects using BSA as a model test protein to synthesize BSA@ZIF-8 NPs at various metal-to-ligand (M:L) ratios. SEM, FTIR, XRD, and DLS were applied to characterize the morphology and structure of BSA@ZIF-8 NPs and their effects on protein loading capacity. Degradation kinetics and protein release behavior of BSA@ZIF-8 NPs were evaluated at pH 5.0 (to simulate the tumor environment) and pH 7.4 (to mimic the blood environment). Our objective was to define optimal combinations of the high protein loading rate and rapid release under varying pH conditions, and we found that (i) the yield of BSA@ZIF-8 NPs decreased as the M:L ratio increased, but the protein content increased. This highlights the need to strike a balance between cost-effectiveness and practicality when selecting ZIF-8 NPs with different molar ratios for protein-based drug formulation. (ii) BSA@ZIF-8 NPs exhibited cruciate flower-like shapes when synthesized using $Zn(NO_3)_2$ as the zinc precursor at M:L ratios of 1:16 or 1:20. In all other cases, the NPs displayed a regular rhombic dodecahedral structure. Notably, the release behavior of the NPs did not differ significantly between these morphologies. (iii) When $Zn(OAc)_2$ was used as the zinc precursor, the synthesized ZIF-8 NPs exhibited a smaller size compared to the $Zn(NO_3)_2$-derived ZIF-8 NPs. (iv) The release rate and amount of BSA protein were higher at pH 5.0 compared to pH 7.4. (v) Among the different formulations, BSA@ZIF-8 with an M:L ratio of 1:16 at pH 5.0 was observed to have a shorter time to reach a plateau (0.5 h) and higher protein release, making it suitable for locally rapid administration in a tumor environment. BSA@ZIF-8 prepared from $Zn(OAc)_2$ at an M:L ratio of 1:140 showed the slower release of BSA protein over a 24-h period, indicating its suitability for sustained release delivery. In conclusion, our findings provide a useful basis for the practical application of ZIF-8 NPs in protein-based drug delivery systems.

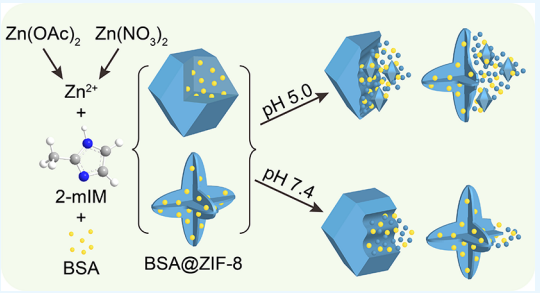

1. INTRODUCTION

Protein drugs (therapeutic proteins) have many advantages: high activity, strong specificity, low toxicity, well-defined biological function, and effective clinical application.[1] Two obstacles to their successful use are low cellular uptake efficiency and rapid clearance by the immune system and enzymatic environment.[2] To overcome these obstacles, various carrier systems have been developed for the encapsulation and delivery of protein drugs, and bovine serum albumin (BSA) is commonly used as a model test protein in these investigations.[3−5]

Zeolitic imidazolate frameworks (ZIFs), a subcategory of metal−organic framework (MOF) materials, are composed of tetrahedral metal ions (particularly Zn^{2+}, Co^{2+}, Cu^{2+}, or Fe^{2+}) ligated to imidazolate groups.[6] One of the best-studied ZIF carriers is ZIF-8, consisting of Zn^{2+} linked to 2-methylimidazole (2-mIM). The advantages of ZIF-8 include high surface area, low cytotoxicity, and chemical and thermal stability in aqueous solution.[7] Chu's group used BSA as a model test protein to create biomineralized protein-encapsulated ZIF-8 nanoparticles (NPs) for intracellular delivery and endolysosomal release of proteins, thereby maintaining activity of the proteins and protecting them from enzyme-mediated degradation.[8] The high biocompatibility and drug loading capacity of ZIF-8 facilitate embedding of a variety of biomolecules (e.g., enzymes, DNA, and proteins), such that leakage is reduced and biological activity is maintained.[9−11] Even more, ZIF-8 exhibits pH-dependent release behaviors that are crucial for drug delivery within living organisms. It undergoes degradation in acidic conditions (pH 5.0−6.0), thereby enabling the effective delivery and release of a carrier that can be controlled by the pH level.[12−14]

Received: July 12, 2023
Revised: August 16, 2023
Accepted: November 3, 2023
Published: November 16, 2023

ZIF-8 synthesis is affected by factors such as the metal ion source and molecular structure of organic ligands, and ZIF-8 framework structures are affected by the molar ratio, reaction time, stirring rate, and solvent used. Beh et al. found that increasing the Zn^{2+} concentration alone promoted the ZIF-8 nucleation while suppressed the ZIF-8 nucleus growth to result in smaller ZIF-8 particles (<200 nm).[15] On the other hand, mechanical stirring is another key factor in ZIF-8 manufacturing, as static synthetic conditions resulted in slightly larger crystallites compared to those formed in mechanically stirred reactions (1.58 ± 0.15 μm versus 1.33 ± 0.14 μm).[16] The hydrogen bond donation ability of a solvent, which determines the crystallization rate and nanocrystal size, is a primary factor affecting the ZIF-8 synthesis process.[17] Studies of ZIF-8 synthesis and crystallinity under varying zinc sources, molar ratios, and water contents demonstrated that the particle size and shape can be controlled by adjusting the 2-mIM concentration.[18] Polycrystalline or amorphous products may be formed during ZIF-8 synthesis as a result of reactions involving imidazolate ligands, adversely affecting the production and encapsulation of protein drugs.

Few studies have examined in detail the effects of Zn^{2+} sources and molar ratios on synthesis and encapsulation efficiency of ZIF-8 loaded with protein drugs.[19] ZIF-8 has strong thermal and chemical stability[20], but reacts rapidly in acidic (low pH) environments. This is a result of the protonation of organic ligands in such environments, leading to cleavage of Zn−N bonds, breakdown of the ZIF-8 skeleton, and consequent release of the drug.[21] Falcaro's group analyzed structural and chemical changes of pure ZIF-8 particles exposed to the PBS medium and demonstrated more rapid degradation of smaller particles.[22] ZIF-8 microcrystals were shown by Morozov's group to be more strongly degraded by a PBS solution with pH 7.4 than by a lactic acid solution with pH 5.0.[23] There have been no systematic studies, to date, on stability of protein encapsulation of ZIF-8 NPs, or their releasing behaviors, in relation to protein loading capacity, crystal size, or environmental pH. Understanding such relationships is important for design of *in vitro* and *in vivo* experiments.

To elucidate such relationships, we systematically investigated BSA@ZIF-8 synthesis under various metal-to-ligand (M:L) ratios, with BSA as a test protein. We used three complementary approaches: (i) study effects of two common zinc sources (zinc nitrate and zinc acetate) and four Zn:2-mIM molar ratios (1:16, 1:20, 1:30, and 1:140) on the BSA@ZIF-8 NPs formation process, (ii) characterize (by several techniques) the BSA@ZIF-8 morphology and structure and roles of these factors in determining the protein drug loading rate, and (iii) analyze BSA@ZIF-8 degradation kinetics and protein release behavior in simulated tumor (pH 5.0) and blood (pH 7.4) physiological environments. Our overall objective was to define optimal combinations of high protein loading rates and rapid release under varying pH conditions.

2. EXPERIMENTAL SECTION

2.1. Materials. Zinc acetate dihydrate [$Zn(OAc)_2{\cdot}2H_2O$] and zinc nitrate hexahydrate [$Zn(NO_3)_2{\cdot}6H_2O$] were purchased from Sinopharm Chemical Reagent Co. (Shanghai). 2-Methylimidazole (2-mIM) and lactic acid were from Shanghai Aladdin Biochemical Technology Co. (Shanghai). BSA (purity of ≥97%) was from Shanghai Lanji Technology Development Co. (Shanghai). Saline solution (0.9%) was from Sichuan Kelun Pharmaceutical Co. (Chengdu). PBS buffer was from OriGene Technologies, Inc. (Wuxi). The bicinchoninic acid (BCA) protein assay kit, SDS-PAGE Gel Fast Preparation Kit, and Fast Silver Stain Kit were from Beyotime Biotechnology Co. (Shanghai). All chemical reagents were used without further purification.

2.2. Synthesis of ZIF-8 and BSA@ZIF-8. For synthesis of ZIF-8, 0.2 mmol of $Zn(OAc)_2{\cdot}2H_2O$ was dissolved in 1 mL of deionized (DI) water, and 6 mmol of 2-mIM was dissolved in 3 mL of DI water.[24] For synthesis of BSA@ZIF-8, 2 mg of BSA was dissolved in 1 mL of 0.9% saline solution to prepare stock solutions, 6 mmol of 2-mIM was dissolved in 2 mL of DI water, and 1 mL of stock solution was added at room temperature. The above solutions were added dropwise with Zn^{2+} solution and stirred for 1 h at room temperature. NPs were collected by centrifugation (10,000 rpm, 10 min), washed 3× with DI water (10,000 rpm, 5 min), and lyophilized for 12 h. Supernatants were collected for BCA protein assays to determine protein encapsulation efficiency. The 2-mIM/Zn molar ratio was adjusted to 16, 20, and 140 for investigation of effects on product synthesis.[25,26] Synthesis of ZIF-8 and BSA@ZIF-8 using $Zn(NO_3)_2$ was performed by a procedure analogous to that using $Zn(OAc)_2$.

2.3. Characterization of ZIF-8 and BSA@ZIF-8. *2.3.1. Morphology.* Scanning electron microscopy (SEM) (model S-4800, Hitachi High-Tech Corp.; Tokyo) was used to study the morphology. For both carriers, a test sample was dispersed in a small amount of anhydrous ethanol, and a single drop was placed on a monocrystalline silicon wafer and dried in a desiccator for 10 min. The dried sample was gold-covered by an ion sputtering device (model E1010, Hitachi) (pressure: 8×10^{-4} Mbar; current: 25 mA) and observed by SEM.[27]

2.3.2. Dynamic Light Scattering (DLS). Samples were placed in microcentrifuge tubes and suspended in DI water. 3 mL of the suspension was placed in a cuvette and read in a Beckman Coulter Delsa Nano C to estimate the average particle size.[28]

2.3.3. X-ray Diffraction Analysis (XRD). XRD patterns were obtained using a D8 Advance diffractometer (Bruker; Germany). Samples were run using Cu Kα radiation (λ = 1.5418 A) under continuous mode scanning, a rate of 2°/min, and a temperature range of 5−60°.[29]

2.3.4. Fourier Transform Infrared Spectroscopy (FTIR). Functional groups were determined by analyzing infrared spectra on a spectrometer (model IS10, Thermo Fisher Scientific; USA). Samples were ground gently with KBr in a mortar and compressed into transparent sheets (pressure: 400 kg/cm^2), and scans were taken over the frequency range of 4,000 to 400 cm^{-1}.[30]

2.4. Release of BSA@ZIF-8 at Two pH Values. A release system was prepared by suspending BSA@ZIF-8 NPs in PBS buffer (pH 5.0 or 7.4) at a concentration of 10 mg/mL, shaking (200 rpm, 37 °C) in an intelligent shaking incubator, and centrifuging (15,000 rpm, 2 min) at defined intervals. The supernatant was collected, stored at 4 °C, and added with an equal volume of fresh buffer solution for subsequent experiments. Then lactic acid (LA), NaCl solution with lactic acid, saline solution, and DMEM were used as buffer according to the above release study method.

2.5. Released BSA Protein Assay. *2.5.1. BCA Protein Assay.* The concentration of released BCA proteins was determined using the BCA protein assay kit. The amount of BSA protein released from BSA@ZIF-8 was calculated based on the volume of the collected supernatant and used to determine the rate of protein release.

https://doi.org/10.1021/acsomega.3c04973
ACS Omega 2023, 8, 44601−44610

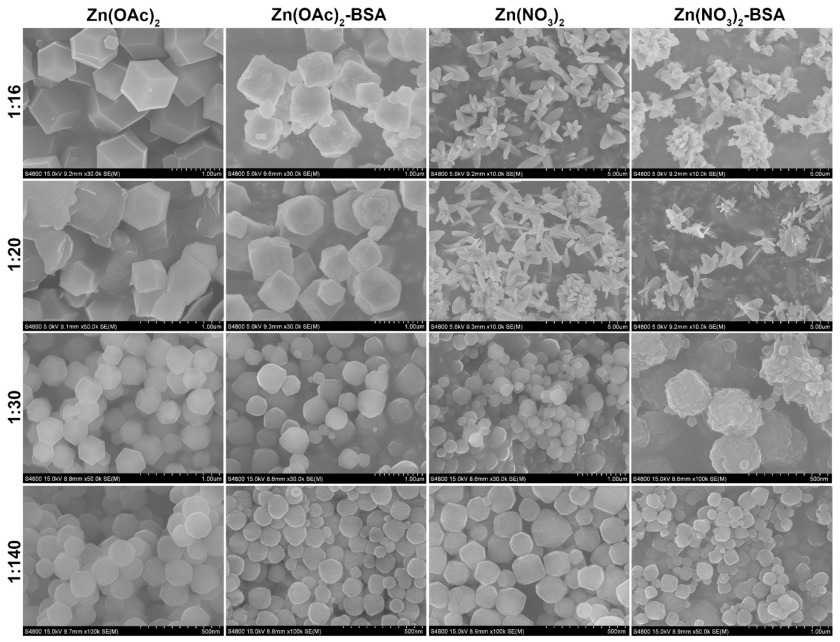

Figure 1. SEM images of ZIF-8 and BSA@ZIF-8 NPs synthesized using four different zinc precursors (top) and four different M:L ratios (left).

2.5.2. SDS-PAGE and Silver Staining. 20 μL of protein was loaded onto 10% gel and subjected to SDS-PAGE (80 V for 30 min, 120 V for 1 h), and the gel was stained using a Fast Silver Stain Kit.

2.6. Statistical Analysis. All experiments were performed in triplicate (n = 3). The software program GraphPad Prism was used for data analysis and graph generation. Means were compared by Dunnett's test.

3. RESULTS AND DISCUSSION

3.1. Synthesis and Characterization of BSA@ZIF-8 Crystals. The morphology of ZIF-8 and BSA@ZIF-8 NPs synthesized using different Zn^{2+}/2-mIM ratios was examined by using SEM (Figure 1). When $Zn(OAc)_2$ was used as a zinc precursor, the synthesized ZIF-8 NPs displayed a regular rhombic dodecahedral structure, whereas BSA@ZIF-8 NPs had blurred edges and uneven surfaces, as observed in previous studies.[5,31,32] When $Zn(NO_3)_2$ was used as the precursor, the morphology varied depending on the M:L ratio. For instance, at M:L ratios of 1:16 or 1:20, BSA@ZIF-8 nanoparticles partially aggregated into cruciate flower-like shapes. At M:L ratios of 1:30 or 1:140, ZIF-8 nanoparticles had rough spheroidal shapes. This morphological variability may be attributed to the strong coordination interaction between Zn^{2+} and 2-mIM.[33]

Particle sizes and distribution ranges of the samples were evaluated by using DLS, and the corresponding results are presented in Figure 2. When $Zn(OAc)_2$ was used as the zinc precursor, the synthesized ZIF-8 NPs exhibited a smaller size range of 69−657 nm compared to the $Zn(NO_3)_2$-derived ZIF-8 NPs, which ranged from 165 to 719 nm (Figure S1). Interestingly, upon loading of blank ZIF-8 nanoparticles with BSA, their size exhibited a general increase. Notably, when zinc ions ($Zn(OAc)_2$) and imidazole were used at a molar ratio of 1:20, the resulting nanoparticles reached a size of up to 1134 nm. However, we also found that BSA@ZIF-8 synthesized from $Zn(OAc)_2$ at an M:L ratio of 1:30 still kept a small size (268.5 nm). These findings provide useful insights for optimizing conditions for synthesis and application of BSA@ZIF-8 with a

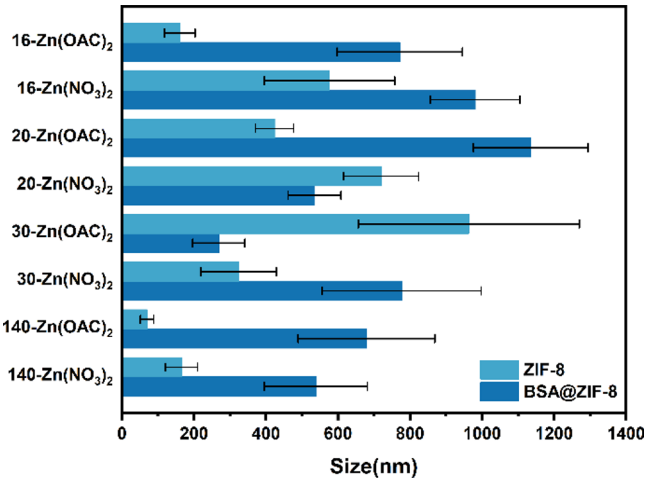

Figure 2. Average sizes of ZIF-8 and BSA@ZIF-8 NPs synthesized using various combinations of zinc precursors and M:L ratios as indicated on the Y-axis.

defined morphology and particle size. For example, dispersity of NPs in the size range of 100−300 nm is suitable for intravenous or oral delivery.[34,35] Particles in the size range of 300 nm to 1 μm can be deposited or endocytosed in certain parts of the respiratory system, e.g., those <500 nm in lung endothelial cells and those >500 nm in the alveolar region.[36] Particles with a size of roughly 1 μm may enter blood circulation via intranasal administration.[37,38]

XRD patterns of ZIF-8 and BSA@ZIF-8 are shown in Figure 3A and Figure S3. In comparisons of XRD patterns, peaks of ZIF-8 from $Zn(NO_3)_2$ at ratios of 1:16 and1:20 were similar to those of simulated cruciate flower-like ZIF-L (Figure S2).[39] ZIF-8 from $Zn(NO_3)_2$ at ratios of 1:30 and 1:140 and from $Zn(OAc)_2$ displayed reflection along the planes (011), (002), and (013) (respectively at 7.33, 10.37, and 12.71°), which were consistent with the characteristic peaks similar to those of simulated rhombic dodecahedral ZIF-8 (Figure S2).[40] Characteristic peaks of BSA@ZIF-8 were consistent with those of ZIF-

https://doi.org/10.1021/acsomega.3c04973
ACS Omega 2023, 8, 44601−44610

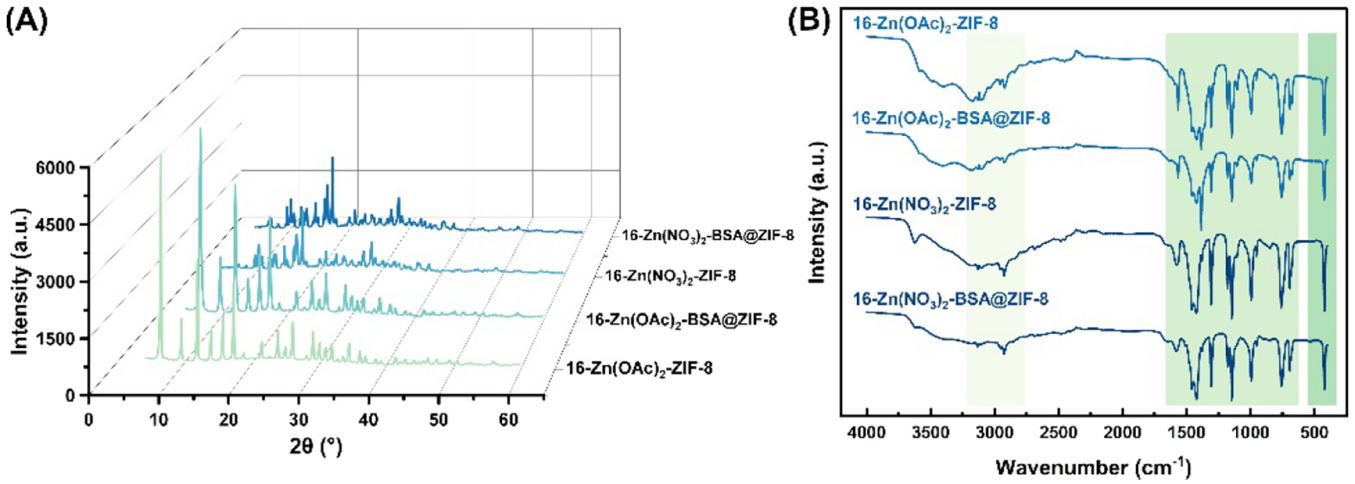

Figure 3. (A) XRD patterns and (B) FTIR spectra of ZIF-8 and BSA@ZIF-8 NPs prepared from various zinc precursors at the M:L ratio of 1:16.

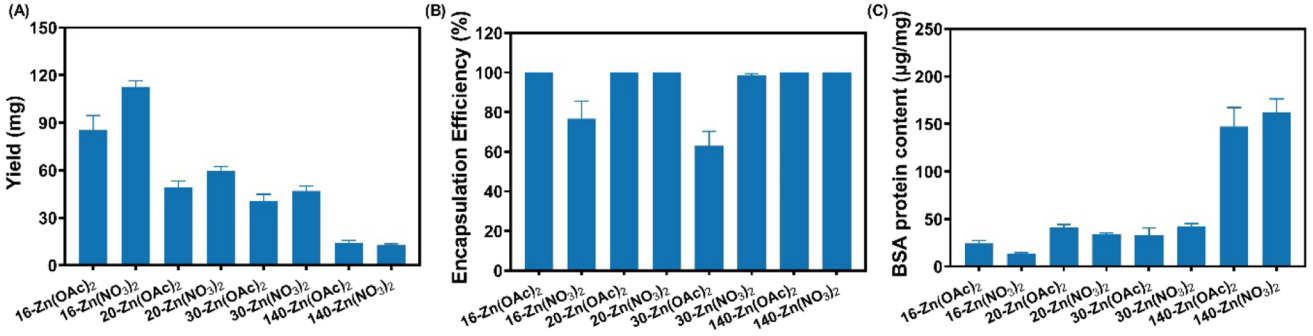

Figure 4. Yield (A), encapsulation efficiency (B), and content (C) of BSA@ZIF-8 NPs prepared from various zinc precursors at various M:L ratios as indicated.

8, indicating that the ZIF-8 crystal structure was unaffected by the loading process and remained intact. The increase in BSA@ZIF-8 intensity values confirmed that BSA was encapsulated in ZIF-8 pores. By importing diffraction patterns collected using Cu Kα radiation, we used a web application named ZIF phase analysis to further identify the crystalline phases.[41] The crystals from $Zn(NO_3)_2$ at ratios of 1:16 and 1:20 belonged to the ZIF-L structure. Nevertheless, the other samples had a pure sodalite crystalline structure like ZIF-8. The XRD data confirmed that BSA@ZIF-8 NPs synthesized using various zinc precursors at different M:L ratios retained the same crystalline form as the pure ZIF-8 NPs, suggesting that BSA protein was successfully encapsulated in ZIF-8 crystals.

The chemical structure and functional group of ZIF-8 crystals and encapsulation of BSA were further studied by the FTIR spectrum (Figure 3B and Figure S4). In the ZIF-8 spectrum, absorption peaks at 3133 and 2920 cm^{-1} corresponded respectively to the aromatic and aliphatic C−H stretching vibrations of the imidazole ring, and the peak at 1562 cm^{-1} resulted from the C═N stretching vibration in the imidazole ring. Broad absorption peaks in the 1475−990 cm^{-1} range corresponded to the C−H bond bending vibrations and C−C single bond skeleton vibrations. Broad peaks at 750 and 684 cm^{-1} corresponded to the out-of-plane ring bending vibration of the imidazole ring. The 419 cm^{-1} peak resulted from Zn−N stretching, a distinctive feature of ZIF-8 integrity.[42] The spectrum of BSA@ZIF-8 NPs exhibited FTIR spectra similar to that of pristine ZIF-8, but reduced peak intensity was reduced relative to ZIF-8. After the loading of the BSA protein, the new characteristic peaks at 1720−1535 cm^{-1} agreeing with amide bands of BSA were observed in the BSA@ZIF-8 FTIR spectrum, confirming the successful encapsulation of BSA within the ZIF-8 nanoparticles. The above findings reflect the successful synthesis of ZIF-8 and encapsulation of BSA in the ZIF-8 framework.

3.2. NP Yield, Content, and BSA Encapsulation Efficiency. The same amount of BSA protein (2 mg) was added for the various zinc precursors and M:L ratios in the synthesis experiments. As the M:L ratio decreased from 1:140 to 1:16, BSA@ZIF-8 yield gradually increased (Figure 4A). For a given ratio, the yield was consistently lower for BSA@ZIF-8 synthesized with $Zn(OAc)_2$ as a precursor, vs $Zn(NO_3)_2$. In particular, the relative yield was much lower for the ratio of 1:140, possibly because excess 2-mIM was adsorbed onto the particle surface and inhibited further growth.[43] For both $Zn(OAc)_2$ and $Zn(NO_3)_2$, the M:L ratio of 1:16 groups achieved the highest yield, reaching 85 and 113 mg, respectively. While the particle size of ZIF-8 impacts its potential for various applications, such as drug delivery, the product yield is equally crucial as it determines the quantity of harvestable ZIF-8 particles available for utilization.[15] It is well-established that the size of the nanoparticles significantly affects their recovery during centrifugation. Additionally, maintaining an appropriate reactant concentration is crucial for achieving high reaction yield and solid yield.[15] This partially explains why the M:L ratio of 1:16 groups exhibited a high yield, as the sizes of nanoparticles reached 771 and 980 nm in the $Zn(OAc)_2$ and $Zn(NO_3)_2$ engaged groups, respectively (Figure S1).

https://doi.org/10.1021/acsomega.3c04973
ACS Omega 2023, 8, 44601−44610

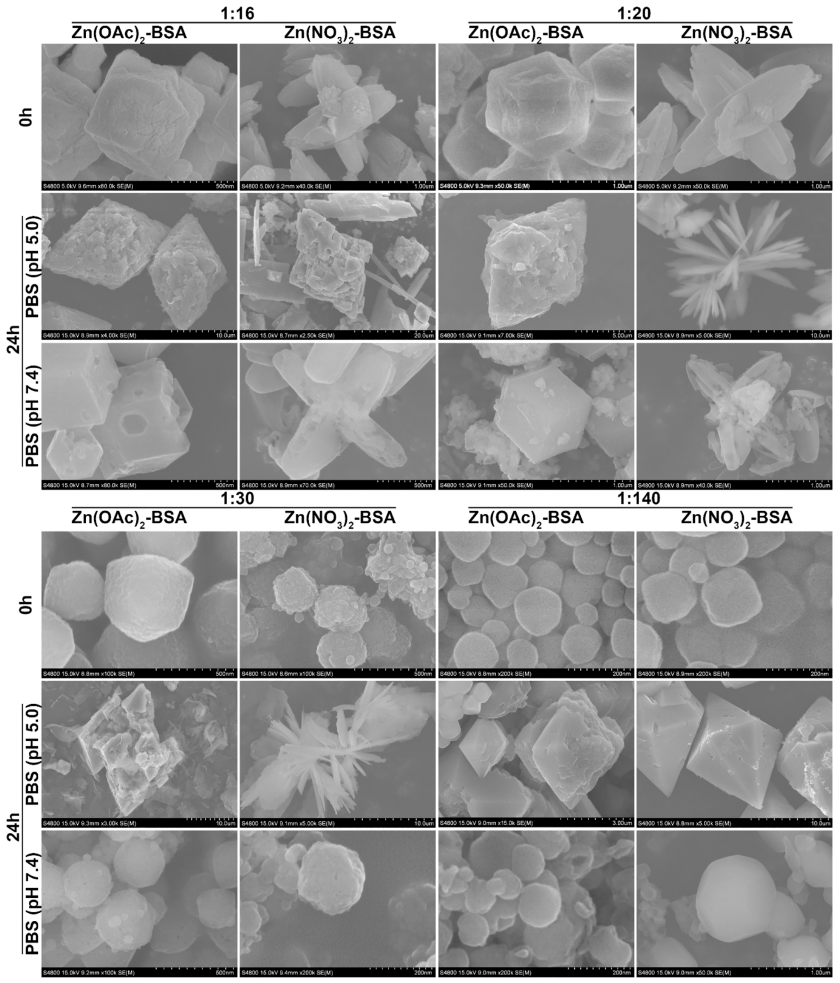

Figure 5. SEM images of BSA@ZIF-8 NPs before and after 24 h of incubation in pH 5.0 and 7.4 PBS solutions.

ZIF-8-based biocomposites spontaneously form in water and primarily consist of Zn^{2+} and 2-mIM, allowing them to attract and encapsulate negatively charged biomacromolecules such as proteins.[44] This biomimetic mineralization process closely resembles natural biomineralization and exhibits impressive encapsulation efficiencies (EE%) for biomacromolecules, typically ranging from 80 to 100%.[45−48] In our study, we quantified the encapsulation efficiency using the BCA protein assay to determine the residual BSA concentration in the supernatant after crystal formation and removal through centrifugation, which generally fell within the range of 60−100% (Figure 4B). Most groups displayed complete BSA encapsulation (100%), with the exception of $Zn(NO_3)_2$ ratio 1:16 and $Zn(OAc)_2$ ratio 1:30 groups (76 and 62%, respectively). On the other hand, we found that the loaded drug (BSA) content differed among groups. The group with the highest M:L ratio (1:140) had the highest BSA content, nearly three times the values observed for other groups (Figure 4C). Nanocarriers having high drug loading capacities provide enhanced delivery of licensed drugs, by extending circulation times, improving drug dissolution rates and bioavailability, and inhibiting rapid clearance of drugs through metabolism.[49] Although the 1:140 M:L groups had relatively low yields (12−14 mg), they had a high protein loading content, a promising feature for *in vivo* applications. Consideration of both cost-effectiveness and practicality is important in choosing among ZIF-8 NPs of varying molar ratios for formulation of protein-based drugs.

3.3. Degradation of BSA@ZIF-8 in PBS. We selected PBS as an isotonic solution that simulates pH, osmolarity, and ion concentrations in the human body.[22] Our testing design involved pH values (5.0 and 7.4) that approximate values in the human tumor and blood.[50] SEM images of BSA@ZIF-8 NPs before and after 24 h of incubation in pH 5.0 and 7.4 PBS solutions (Figure 5) reveal striking morphological changes in pH 5.0 solution. BSA@ZIF-8 underwent clear degradation and production of hexagonal bipyramidal crystals, possibly $Zn_3(PO_4)_2$ (zinc phosphate). These findings were consistent with those of Morozov's group,[23] who observed that interaction of ZIF-8 with PBS resulted in formation of $Zn_3(PO_4)_2$ crystals having some typical dendritic structures that often appear at zinc-containing reactive interfaces. In our study, this phenomenon was most notable for BSA@ZIF-8 synthesized using $Zn(NO_3)_2$ at the M:L ratio of 1:140. In contrast, the initial morphology was retained for BSA@ZIF-8 NPs incubated for 24 h in pH 7.4 PBS. The crystal surface became rough and porous in this case, indicating slower degradation of BSA@ZIF-8 under physiological conditions. This phenomenon was observed for both the rhombic dodecahedral structure and cruciate flower-like morphology of BSA@ZIF-8.

XRD patterns and FTIR spectra of BSA@ZIF-8 NPs before and after 24 h of incubation in pH 5.0 (acidic) and 7.4 (neutral) PBS solutions are shown in Figure 6 and Figures S5 and S6. We

https://doi.org/10.1021/acsomega.3c04973
ACS Omega 2023, 8, 44601−44610

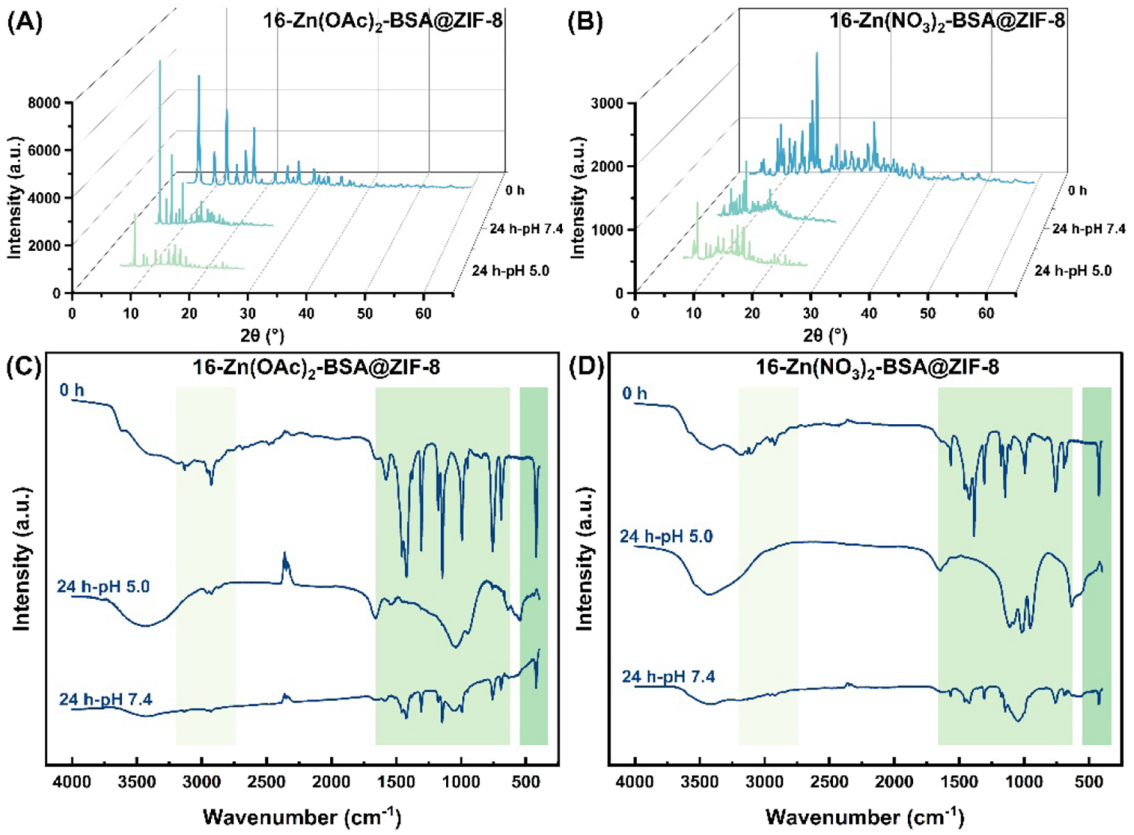

Figure 6. Characteristics of BSA@ZIF-8 NPs (M:L ratio of 1:16) before and after 24 h of incubation in pH 5.0 and 7.4 PBS solutions. (A, B) XRD patterns of NPs prepared from $Zn(OAc)_2$ (A) and from $Zn(NO_3)_2$ (B). (C, D) FTIR spectra of NPs prepared from $Zn(OAc)_2$ (C) and $Zn(NO_3)_2$ (D).

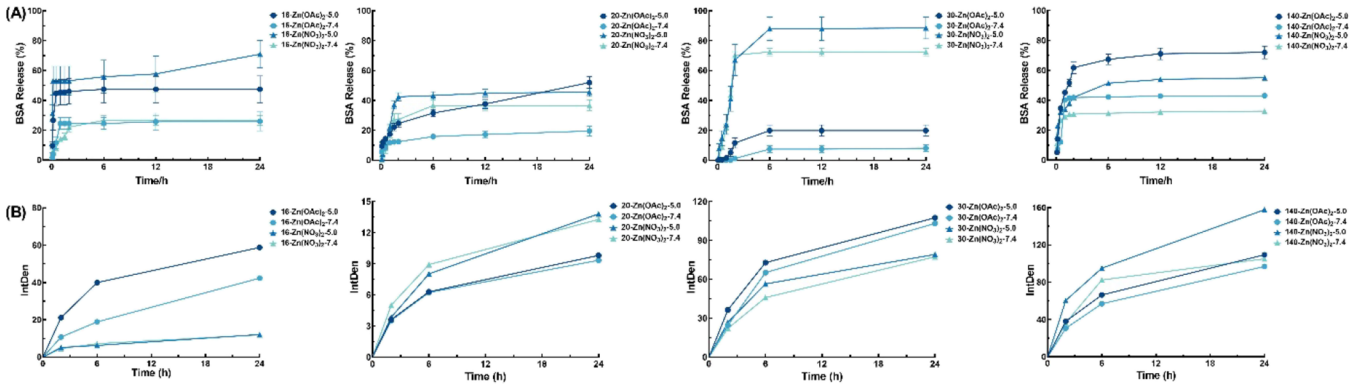

Figure 7. BSA release profiles of BSA@ZIF-8 NPs in pH 5.0 and 7.4 PBS solutions. (A) BCA protein assay. (B) Assay by SDS-PAGE and silver staining.

used "ZIF phase analysis" to analyze the crystalline phases after 24 h of incubation.[41] In a pH 5.0 environment, these BSA@ZIF-8 NPs synthesized with various zinc precursors at different M:L ratios completely collapsed, and the morphology became amorphous. However, after incubation in a pH 7.4 environment for 24 h, the XRD pattern of these BSA@ZIF-8 NPs remained largely unaffected, indicating that the crystallinity of the sample was not significantly altered, which was consistent with the findings of previous research.[51] The above results were consistent with the results acquired by SEM, which proved more destruction of the BSA@ZIF-8 crystal at pH 5.0 than 7.4. FTIR spectra indicated that a 24-h degradation at pH 5.0 left nearly no BSA@ZIF-8-specific bands, and results did not differ notably for the rhombic dodecahedral structure (Figure 6C) vs cruciate flower-like morphology (Figure 6D). Over 24 h of incubation at pH 5.0, the characteristic peaks at 1770−1520 cm^{-1} were obviously observed, which were related to the vibration of an oxygen-containing acyl group in the amide bond, demonstrating the successful release of BSA protein. In contrast, a residual Zn−N stretching vibration at 419 cm^{-1} was observed in both cases at pH 7.4, indicating incomplete BSA@ZIF-8 degradation. Meanwhile, interaction of BSA@ZIF-8 with PBS resulted in the appearance of a new series of bands that confirmed the formation of $Zn_3(PO_4)_2$ species: broad absorption peaks in the 1250−1100 cm^{-1} range corresponded to the P═O bond stretching vibrations, broad peaks in the

https://doi.org/10.1021/acsomega.3c04973
ACS Omega 2023, 8, 44601−44610

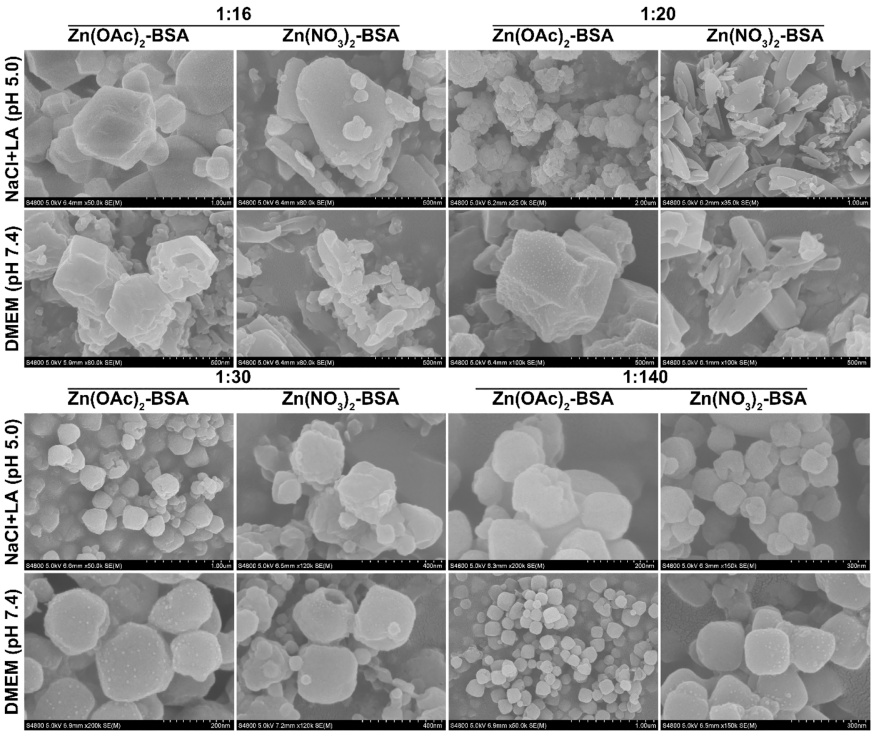

Figure 8. SEM images of BSA@ZIF-8 NPs after 24 h of incubation in NaCl solution with lactic acid (pH 5.0) and DMEM (pH 7.4).

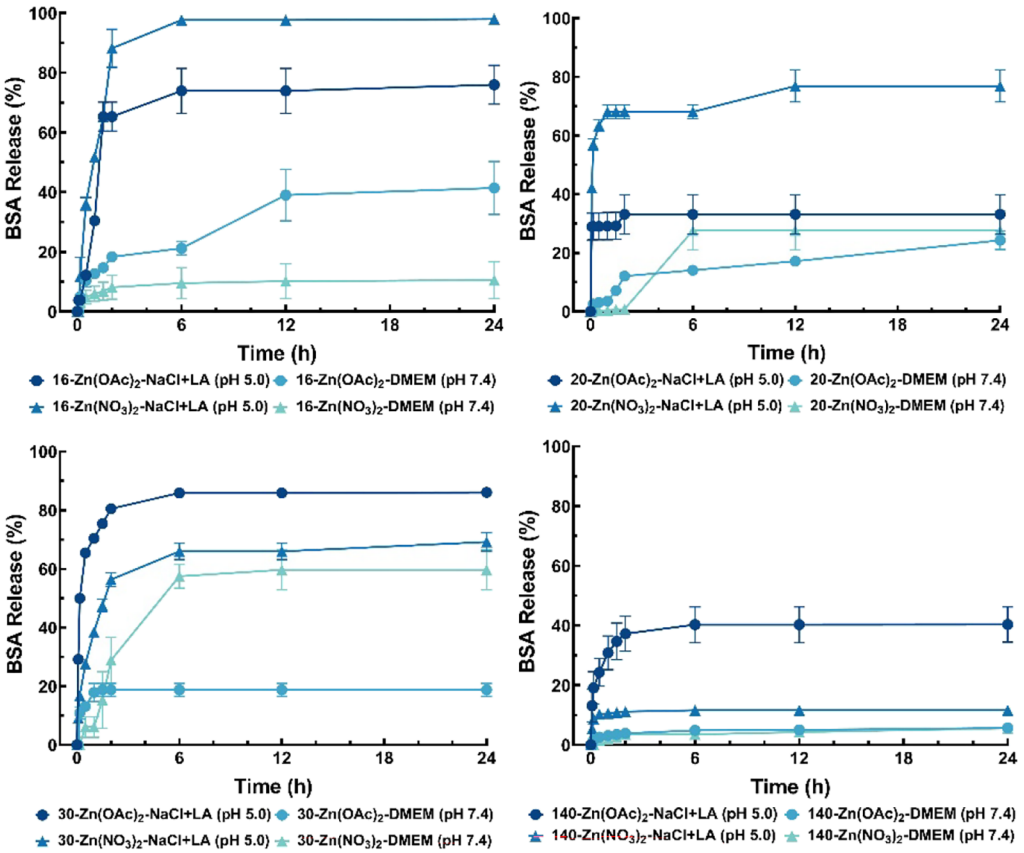

Figure 9. BSA release profiles of BSA@ZIF-8 NPs in NaCl solution with lactic acid (pH 5.0) and DMEM (pH 7.4).

1100−950 cm^{-1} range corresponded to the asymmetric P═O stretching vibrations, the strong peak at 940 cm^{-1} corresponded to the P−O stretching vibration, and broad peaks in the 650−520 cm^{-1} range corresponded to the PO_4^{3-} bending vibrations.

The release of BSA protein from BSA@ZIF-8 was analyzed in pH 5.0 and 7.4 PBS solutions using the BCA protein assay and SDS-PAGE (Figure 7A). Interestingly, there was no significant difference in the release rate between groups with different

https://doi.org/10.1021/acsomega.3c04973
ACS Omega 2023, 8, 44601−44610

nanoparticle sizes and structures, specifically between the rhombic dodecahedral structure and the cruciate flower-like morphology. The environmental pH played a crucial role in the release of the loaded protein, with a higher release rate and amount observed at pH 5.0 compared to pH 7.4. Over a 24-h period, the highest release of BSA protein was observed for BSA@ZIF-8 prepared from $Zn(NO_3)_2$ at an M:L ratio of 1:30, with 88.51% released at pH 5.0 and 72.47% released at pH 7.4, respectively. As the M:L ratio increased from 1:16 to 1:140, the release rate of BSA@ZIF-8 during the first hour increased and reached a plateau value around 2 h in most cases. The shortest time to reach a plateau (0.5 h) was observed for BSA@ZIF-8 with an M:L ratio of 1:16 at pH 5.0. Moreover, our results were further validated by SDS-PAGE and silver staining, as depicted in Figure 7B and Figure S7.

3.4. Degradation of BSA@ZIF-8 in NaCl Solution with Lactic Acid and DMEM. Due to the high secretion of lactic acid by tumor cells, the tumor environment exhibits acidification.[52] In this study, we compared the release of BSA from BSA@ZIF-8 incubated in a solution of NaCl with lactic acid (pH 5.0) and DMEM (pH 7.4) to simulate the tumor and physiological environments, respectively. We also used lactic acid (adjusted to pH 5.0 with $NaHCO_3$) and a 0.9% saline solution (pH 7.0) as control groups for comparison. SEM images of BSA@ZIF-8 NPs after 24 h of incubation in these solutions (Figure 8 and Figure S8) revealed the morphological changes. Similar to the PBS buffer, the morphology of BSA@ZIF-8 underwent varying degrees of change. After incubation in NaCl solution with lactic acid for 24 h, the structure of BSA@ZIF-8 was clearly broken or became wrinkled and porous. However, no $Zn(PO_3)_4$ crystals were observed. Similar observations were made in DMEM and the saline solution, where the morphology of BSA@ZIF-8 became rough, but the original morphology remained visible. These findings suggest that BSA@ZIF-8 degrades faster in an acidic environment compared with a physiological environment, mirroring the behavior observed in the PBS buffer.

As depicted in Figure 9, it is observed that the acid−base degree was the main reason affecting the release of BSA, and the buffer itself did not affect the release trend of BSA@ZIF-8. Taking an M:L ratio of 1:16 as an example, BSA@ZIF-8 NPs synthesized with both $Zn(OAc)_2$ and $Zn(NO_3)_2$ reached a plateau value around 2 h followed by BSA@ZIF-8 prepared from $Zn(NO_3)_2$ that showed a higher release rate with 97.99% than $Zn(OAc)_2$ with 75.95%. Compared with the PBS buffer, the higher BSA protein release amount was observed for BSA@ZIF-8 after 24 h of incubation in NaCl solution with lactic acid. The proposed reason for this phenomenon was that the existence of zinc phosphate formed a protective layer on the surface of BSA@ZIF-8 aggregation, in turn affecting the degradation of BSA@ZIF-8.[22] To further verify the effect of buffer on the release of BSA@ZIF-8 NPs, we investigated the abovementioned release situation of BSA@ZIF-8 NPs in lactic acid and saline solution (Figure S9). It was found that the release rate and amount of BSA@ZIF-8 after incubation in pure lactic acid were higher than those in NaCl solution with lactic acid, which indicated that the concentration of hydrogen bonds in buffer solution was the key factor to determine the release of protein at the same pH value.[23,53]

4. CONCLUSIONS

We successfully synthesized a diverse range of BSA@ZIF-8 nanoparticles and evaluated their release properties at pH 5.0 and 7.4 to simulate the conditions of both tumor and blood environments, respectively. Our findings have significant implications for the practical application of ZIF-8 NPs in protein-based drug delivery systems. The key conclusions are as follows:

1. When $Zn(OAc)_2$ was used as the zinc precursor, the synthesized ZIF-8 NPs exhibited a smaller size compared to the $Zn(NO_3)_2$-derived ZIF-8 NPs. BSA@ZIF-8 NPs exhibited cruciate flower-like shapes when synthesized using $Zn(NO_3)_2$ as the zinc precursor at M:L ratios of 1:16 or 1:20. In all other cases, the NPs displayed a regular rhombic dodecahedral structure.
2. The yield of BSA@ZIF-8 NPs decreased as the M:L ratio increased, but the protein content increased. This highlights the need to strike a balance between cost-effectiveness and practicality when selecting ZIF-8 NPs with different molar ratios for protein-based drug formulation.
3. There was no significant difference in the release rate between BSA@ZIF-8 NPs with different sizes or structures, but the concentration of hydrogen bonds in the buffer solution was the key factor.
4. Among the different formulations, BSA@ZIF-8 with an M:L ratio of 1:16 at pH 5.0 exhibited a shorter time to reach a plateau (0.5 h) and higher protein release, making it suitable for locally rapid administration in a tumor environment. BSA@ZIF-8 prepared from $Zn(OAc)_2$ at an M:L ratio of 1:140 showed the slower release of BSA protein over a 24-h period, indicating its suitability for sustained release delivery.

In summary, our study provides valuable insights into the synthesis and properties of BSA@ZIF-8 NPs for protein-based drug delivery systems, aiding future applications in blood and tumor environments.

■ ASSOCIATED CONTENT

Supporting Information

The Supporting Information is available free of charge at https://pubs.acs.org/doi/10.1021/acsomega.3c04973.

Simulated XRD patterns of ZIF-8 with a rhombic dodecahedral structure and cruciate flower-like morphology; DLS measurement, XRD patterns, and FTIR spectra of ZIF-8 and BSA@ZIF-8 prepared from various zinc precursors at different M:L ratios; XRD patterns and FTIR spectra of BSA@ZIF-8 NPs before and after 24 h of incubation in pH 5.0 and 7.4 PBS solutions, prepared from various zinc precursors at different M:L ratios; BSA release images of BSA@ZIF-8 NPs in pH 5.0 and 7.4 PBS solutions assayed by SDS-PAGE and silver staining; SEM images and BSA release profiles of BSA@ZIF-8 NPs after 24 h of incubation in lactic acid (pH 5.0) and 0.9% NaCl solution (pH 7.0) (PDF)

■ AUTHOR INFORMATION

Corresponding Authors

Wenhui Chu − *Taizhou Key Laboratory of Biomass Functional Materials Development and Application, School of Life Science, Taizhou University, Taizhou, Zhejiang 318000, China;* orcid.org/0009-0005-7694-8249; Email: jake-chu@hotmail.com

Yongqian Fu − *Taizhou Key Laboratory of Biomass Functional Materials Development and Application, School of Life Science,*

https://doi.org/10.1021/acsomega.3c04973
ACS Omega 2023, 8, 44601−44610

Taizhou University, Taizhou, Zhejiang 318000, China; Email: bioengineer@163.com

Authors

Jia Gao − *Taizhou Key Laboratory of Biomass Functional Materials Development and Application, School of Life Science, Taizhou University, Taizhou, Zhejiang 318000, China; College of Life Science and Medicine, Zhejiang Sci-Tech University, Hangzhou, Zhejiang 310018, China*

Xuankai Ding − *Taizhou Key Laboratory of Biomass Functional Materials Development and Application, School of Life Science, Taizhou University, Taizhou, Zhejiang 318000, China; College of Life Science and Medicine, Zhejiang Sci-Tech University, Hangzhou, Zhejiang 310018, China*

Lingzhi Ding − *Taizhou Central Hospital, Taizhou University, Taizhou, Zhejiang 318000, China*

Qing Guo − *School of Biological and Chemical Engineering, Zhejiang University of Science and Technology, Hangzhou, Zhejiang 310023, China*

Complete contact information is available at: https://pubs.acs.org/10.1021/acsomega.3c04973

Author Contributions

The manuscript was written based on contributions from all the authors, and they have all approved the finalized version.

Notes

The authors declare no competing financial interest.

■ ACKNOWLEDGMENTS

This study was supported by the Natural Science Foundation of Zhejiang Province (LTGD23C100001, LBY22H180009, and 2022C02076) and the Pan'an Science and Technology Plan Project (202001). The authors are grateful to Dr. S. Anderson for English editing of the manuscript.

■ REFERENCES

(1) Zhao, N.; Song, Y.; Xie, X.; Zhu, Z.; Duan, C.; Nong, C.; Wang, H.; Bao, R. Synthetic biology-inspired cell engineering in diagnosis, treatment, and drug development. *Signal Transduction Targeted Ther.* **2023**, *8* (1), 112.

(2) Jia, J.; Zhang, S.; Wen, K.; Li, Q. Nano-Scaled Zeolitic Imidazole Framework-8 as an Efficient Carrier for the Intracellular Delivery of RNase A in Cancer Treatment. *Int. J. Nanomedicine* **2019**, *14*, 9971−9981.

(3) Wu, Q.; Li, M.; Tan, L.; Yu, J.; Chen, Z.; Su, L.; Ren, X.; Fu, C.; Ren, J.; Li, L.; Cao, F.; Liang, P.; Zhang, Y.; Meng, X. A tumor treatment strategy based on biodegradable BSA@ZIF-8 for simultaneously ablating tumors and inhibiting infection. *Nanoscale Horiz* **2018**, *3* (6), 606−615.

(4) Abd Al-Jabbar, S.; Atiroglu, V.; Hameed, R. M.; Guney Eskiler, G.; Atiroglu, A.; Deveci Ozkan, A.; Ozacar, M. Fabrication of dopamine conjugated with protein @metal organic framework for targeted drug delivery: A biocompatible pH-Responsive nanocarrier for gemcitabine release on MCF-7 human breast cancer cells. *Bioorg Chem.* **2022**, *118*, No. 105467.

(5) Kumar, P.; Bansal, V.; Paul, A. K.; Bharadwaj, L. M.; Deep, A.; Kim, K. H. Biological applications of zinc imidazole framework through protein encapsulation. *Appl. Nanosci* **2016**, *6* (7), 951−957.

(6) Jia, Q.; Lasseuguette, E.; Lozinska, M. M.; Ferrari, M. C.; Wright, P. A. Hybrid Benzimidazole-Dichloroimidazole Zeolitic Imidazolate Frameworks Based on ZIF-7 and Their Application in Mixed Matrix Membranes for CO(2)/N(2) Separation. *ACS Appl. Mater. Interfaces* **2022**, *14* (41), 46615−46626.

(7) Liu, W.; Wang, F.; Zhu, Y.; Li, X.; Liu, X.; Pang, J.; Pan, W. Galactosylated Chitosan-Functionalized Mesoporous Silica Nanoparticle Loading by Calcium Leucovorin for Colon Cancer Cell-Targeted Drug Delivery. *Molecules* **2018**, *23* (12), 3082 DOI: 10.3390/molecules23123082.

(8) Chen, T. T.; Yi, J. T.; Zhao, Y. Y.; Chu, X. Biomineralized Metal-Organic Framework Nanoparticles Enable Intracellular Delivery and Endo-Lysosomal Release of Native Active Proteins. *J. Am. Chem. Soc.* **2018**, *140* (31), 9912−9920.

(9) Liang, K.; Ricco, R.; Doherty, C. M.; Styles, M. J.; Bell, S.; Kirby, N.; Mudie, S.; Haylock, D.; Hill, A. J.; Doonan, C. J.; Falcaro, P. Biomimetic mineralization of metal-organic frameworks as protective coatings for biomacromolecules. *Nat. Commun.* **2015**, *6*, 7240.

(10) Wu, X.; Ge, J.; Yang, C.; Hou, M.; Liu, Z. Facile synthesis of multiple enzyme-containing metal-organic frameworks in a biomolecule-friendly environment. *Chem. Commun. (Camb)* **2015**, *51* (69), 13408−11.

(11) Lyu, F.; Zhang, Y.; Zare, R. N.; Ge, J.; Liu, Z. One-pot synthesis of protein-embedded metal-organic frameworks with enhanced biological activities. *Nano Lett.* **2014**, *14* (10), 5761−5.

(12) Zhao, Z.; Liu, Z.; Hua, Y.; Pan, Y.; Yi, G.; Wu, S.; He, C.; Zhang, Y.; Yang, Y. Biomimetic ZIF8 Nanosystem With Tumor Hypoxia Relief Ability to Enhance Chemo-Photothermal Synergistic Therapy. *Front Pharmacol* **2022**, *13*, No. 850534.

(13) Liao, F. S.; Lo, W. S.; Hsu, Y. S.; Wu, C. C.; Wang, S. C.; Shieh, F. K.; Morabito, J. V.; Chou, L. Y.; Wu, K. C.; Tsung, C. K. Shielding against Unfolding by Embedding Enzymes in Metal-Organic Frameworks via a de Novo Approach. *J. Am. Chem. Soc.* **2017**, *139* (19), 6530−6533.

(14) Lian, X.; Fang, Y.; Joseph, E.; Wang, Q.; Li, J.; Banerjee, S.; Lollar, C.; Wang, X.; Zhou, H. C. Enzyme-MOF (metal-organic framework) composites. *Chem. Soc. Rev.* **2017**, *46* (11), 3386−3401.

(15) Beh, J. J.; Lim, J. K.; Ng, E. P.; Ooi, B. S. Synthesis and size control of zeolitic imidazolate framework-8 (ZIF-8): From the perspective of reaction kinetics and thermodynamics of nucleation. *Mater. Chem. Phys.* **2018**, *216*, 393−401.

(16) Liang, W. B.; Ricco, R.; Maddigan, N. K.; Dickinson, R. P.; Xu, H. S.; Li, Q. W.; Sumby, C. J.; Bell, S. G.; Falcaro, P.; Doonan, C. J. Control of Structure Topology and Spatial Distribution of Biomacromolecules in Protein@ZIF-8 Biocomposites. *Chem. Mater.* **2018**, *30* (3), 1069−1077.

(17) Bustamante, E. L.; Fernandez, J. L.; Zamaro, J. M. Influence of the solvent in the synthesis of zeolitic imidazolate framework-8 (ZIF-8) nanocrystals at room temperature. *J. Colloid Interface Sci.* **2014**, *424*, 37−43.

(18) Jian, M.; Liu, B.; Liu, R.; Qu, J.; Wang, H.; Zhang, X. Water-based synthesis of zeolitic imidazolate framework-8 with high morphology level at room temperature. *RSC Adv.* **2015**, *5* (60), 48433−48441.

(19) Liu, X. L.; Yin, Q.; Huang, G.; Liu, T. F. Stable pyrazolate-based metal-organic frameworks for drug delivery. *Inorg. Chem. Commun.* **2018**, *94*, 21−26.

(20) Wang, S.; Zhang, S. Study on the Structure Activity Relationship of ZIF-8 Synthesis and Thermal Stability. *Journal of Inorganic and Organometallic Polymers and Materials* **2017**, *27* (5), 1317−1322.

(21) Han, C.; Zhang, C. Y.; Tyminska, N.; Schmidt, J. R.; Sholl, D. S. Insights into the Stability of Zeolitic Imidazolate Frameworks in Humid Acidic Environments from First-Principles Calculations. *J. Phys. Chem. C* **2018**, *122* (8), 4339−4348.

(22) Velasquez-Hernandez, M. D.; Ricco, R.; Carraro, F.; Limpoco, F. T.; Linares-Moreau, M.; Leitner, E.; Wiltsche, H.; Rattenberger, J.; Schrottner, H.; Fruhwirt, P.; Stadler, E. M.; Gescheidt, G.; Amenitsch, H.; Doonan, C. J.; Falcaro, P. Degradation of ZIF-8 in phosphate buffered saline media. *CrystEngComm* **2019**, *21* (31), 4538−4544.

(23) Butonova, S. A.; Ikonnikova, E. V.; Sharsheeva, A.; Chernyshov, I. Y.; Kuchur, O. A.; Mukhin, I. S.; Hey-Hawkins, E.; Vinogradov, A. V.; Morozov, M. I. Degradation kinetic study of ZIF-8 microcrystals with and without the presence of lactic acid. *RSC Adv.* **2021**, *11* (62), 39169−39176.

(24) Yuan, M.; Liang, S.; Zhou, Y.; Xiao, X.; Liu, B.; Yang, C.; Ma, P.; Cheng, Z.; Lin, J. A Robust Oxygen-Carrying Hemoglobin-Based

Natural Sonosensitizer for Sonodynamic Cancer Therapy. *Nano Lett.* **2021**, *21* (14), 6042−6050.
(25) Gao, S.; Hou, J. W.; Deng, Z. Y.; Wang, T. S.; Beyer, S.; Buzanich, A. G.; Richardson, J. J.; Rawal, A.; Seidel, R.; Zulkifli, M. Y.; Li, W. W.; Bennett, T. D.; Cheetham, A. K.; Liang, K.; Chen, V. Improving the Acidic Stability of Zeolitic Imidazolate Frameworks by Biofunctional Molecules. *Chem-Us* **2019**, *5* (6), 1597−1608.
(26) Yang, H.; Yu, Z.; Ji, S.; Yan, J.; Han, L.; Liu, Y.; Wang, Y.; Niu, Y.; Huo, Q.; Xu, M. Construction and evaluation of detachable bone-targeting MOF carriers for the delivery of proteasome inhibitors. *RSC Adv.* **2022**, *12* (23), 14707−14715.
(27) Du, L.; Xu, S.; Wu, H.; Zhao, T.; Wang, X.; Wang, M. Facile Fabrication of Diatomite-Supported ZIF-8 Composite for Solid-Phase Extraction of Benzodiazepines in Urine Samples Prior to High-Performance Liquid Chromatography. *Molecules* **2021**, *26* (17), 5209 DOI: 10.3390/molecules26175209.
(28) Zhu, Y.; Yao, Z.; Liu, Y.; Zhang, W.; Geng, L.; Ni, T. Incorporation of ROS-Responsive Substance P-Loaded Zeolite Imidazolate Framework-8 Nanoparticles into a Ca(2+)-Cross-Linked Alginate/Pectin Hydrogel for Wound Dressing Applications. *Int. J. Nanomedicine* **2020**, *15*, 333−346.
(29) Escorihuela, J.; Sahuquillo, Ó.; García-Bernabé, A.; Giménez, E.; Compañ, V. Phosphoric Acid Doped Polybenzimidazole (PBI)/Zeolitic Imidazolate Framework Composite Membranes with Significantly Enhanced Proton Conductivity under Low Humidity Conditions. *Nanomaterials* **2018**, *8* (10), 775 DOI: 10.3390/nano8100775.
(30) Zhang, H.; Shi, X.; Li, J.; Kumar, P.; Liu, B. Selective Dye Adsorption by Zeolitic Imidazolate Framework-8 Loaded UiO-66-NH_2. *Nanomaterials* **2019**, *9* (9), 1283 DOI: 10.3390/nano9091283.
(31) Duan, X.; Luo, Y.; Zhang, R.; Zhou, H.; Xiong, W.; Li, R.; Huang, Z.; Luo, L.; Rong, S.; Li, M.; He, Y.; Ye, Q. ZIF-8 as a protein delivery system enhances the application of dental pulp stem cell lysate in anti-photoaging therapy. *Mater. Today Adv.* **2023**, *17*, No. 100336, DOI: 10.1016/j.mtadv.2022.100336.
(32) Zheng, J.; Li, B.; Ji, Y.; Chen, Y.; Lv, X.; Zhang, X.; Linhardt, R. J. Prolonged release and shelf-life of anticoagulant sulfated polysaccharides encapsulated with ZIF-8. *Int. J. Biol. Macromol.* **2021**, *183*, 1174−1183.
(33) Cui, J.; Feng, Y.; Lin, T.; Tan, Z.; Zhong, C.; Jia, S. Mesoporous Metal-Organic Framework with Well-Defined Cruciate Flower-Like Morphology for Enzyme Immobilization. *ACS Appl. Mater. Interfaces* **2017**, *9* (12), 10587−10594.
(34) Kalani, M.; Yunus, R. Application of supercritical antisolvent method in drug encapsulation: a review. *Int. J. Nanomedicine* **2011**, *6*, 1429−42.
(35) Gigliobianco, M. R.; Casadidio, C.; Censi, R.; Di Martino, P. Nanocrystals of Poorly Soluble Drugs: Drug Bioavailability and Physicochemical Stability. *Pharmaceutics* **2018**, *10* (3), 134 DOI: 10.3390/pharmaceutics10030134.
(36) Pirooznia, N.; Hasannia, S.; Lotfi, A. S.; Ghanei, M. Encapsulation of alpha-1 antitrypsin in PLGA nanoparticles: in vitro characterization as an effective aerosol formulation in pulmonary diseases. *J. Nanobiotechnol.* **2012**, *10*, 20.
(37) Huang, Y.; Donovan, M. D. Large molecule and particulate uptake in the nasal cavity: the effect of size on nasal absorption. *Adv. Drug Deliv Rev.* **1998**, *29* (1−2), 147−155.
(38) Patel, A.; Patel, M.; Yang, X.; Mitra, A. K. Recent advances in protein and Peptide drug delivery: a special emphasis on polymeric nanoparticles. *Protein Pept Lett.* **2014**, *21* (11), 1102−20.
(39) Zhong, L.; Feng, Y.; Hu, H.; Xu, J.; Wang, Z.; Du, Y.; Cui, J.; Jia, S. Enhanced enzymatic performance of immobilized lipase on metal organic frameworks with superhydrophobic coating for biodiesel production. *J. Colloid Interface Sci.* **2021**, *602*, 426−436.
(40) Butt, F. S.; Lewis, A.; Rea, R.; Mazlan, N. A.; Chen, T.; Radacsi, N.; Mangano, E.; Fan, X.; Yang, Y.; Yang, S.; Huang, Y. Highly-Controlled Soft-Templating Synthesis of Hollow ZIF-8 Nanospheres for Selective CO(2) Separation and Storage. *ACS Appl. Mater. Interfaces* **2023**, *15* (26), 31740−31754.
(41) Hafner, M. R.; Villanova, L.; Carraro, F. App-based quantification of crystal phases and amorphous content in ZIF biocomposites. *CrystEngComm* **2022**, *24* (41), 7266−7271.
(42) Zhu, Y.; Zhi, Q.; Zhang, C.; Gu, Y.; Liu, S.; Qiao, S.; Lai, H. Debridement of contaminated implants using air-polishing coupled with pH-responsive maximin H5-embedded metal-organic frameworks. *Front. Bioeng. Biotechnol.* **2023**, *11*, 1124107.
(43) Zhang, Y.; Jia, Y.; Li, M.; Hou, L. Influence of the 2-methylimidazole/zinc nitrate hexahydrate molar ratio on the synthesis of zeolitic imidazolate framework-8 crystals at room temperature. *Sci. Rep.* **2018**, *8*, 9597 DOI: 10.1038/s41598-018-28015-7.
(44) Maddigan, N. K.; Tarzia, A.; Huang, D. M.; Sumby, C. J.; Bell, S. G.; Falcaro, P.; Doonan, C. J. Protein surface functionalisation as a general strategy for facilitating biomimetic mineralisation of ZIF-8. *Chem. Sci.* **2018**, *9* (18), 4217−4223.
(45) Astria, E.; Thonhofer, M.; Ricco, R.; Liang, W. B.; Chemelli, A.; Tarzia, A.; Alt, K.; Hagemeyer, C. E.; Rattenberger, J.; Schroettner, H.; Wrodnigg, T.; Amenitsch, H.; Huang, D. M.; Doonan, C. J.; Falcaro, P. Carbohydrates@MOFs. *Mater. Horiz* **2019**, *6* (5), 969−977.
(46) Liang, K.; Ricco, R.; Doherty, C. M.; Styles, M. J.; Bell, S.; Kirby, N.; Mudie, S.; Haylock, D.; Hill, A. J.; Doonan, C. J.; Falcaro, P. Biomimetic mineralization of metal-organic frameworks as protective coatings for biomacromolecules. *Nat. Commun.* **2015**, *6*, 7240 DOI: 10.1038/ncomms8240.
(47) Chen, T. T.; Yi, J. T.; Zhao, Y. Y.; Chu, X. Biomineralized Metal-Organic Framework Nanoparticles Enable Intracellular Delivery and Endo-Lysosomal Release of Native Active Proteins. *J. Am. Chem. Soc.* **2018**, *140* (31), 9912−9920.
(48) Carraro, F.; Velasguez-Hernandez, M. D.; Astria, E.; Liang, W.; Twight, L.; Parise, C.; Ge, M.; Huang, Z.; Ricco, R.; Zou, X.; Villanova, L.; Kappe, C. O.; Doonan, C.; Falcaro, P. Phase dependent encapsulation and release profile of ZIF-based biocomposites. *Chem. Sci.* **2020**, *11* (13), 3397−3404.
(49) Edagwa, B.; McMillan, J.; Sillman, B.; Gendelman, H. E. Long-acting slow effective release antiretroviral therapy. *Expert Opin Drug Deliv* **2017**, *14* (11), 1281−1291.
(50) Díez-Pascual, A. M.; Rahdar, A. LbL Nano-Assemblies: A Versatile Tool for Biomedical and Healthcare Applications. *Nanomaterials* **2022**, *12* (6), 949 DOI: 10.3390/nano12060949.
(51) Luzuriaga, M. A.; Benjamin, C. E.; Gaertner, M. W.; Lee, H.; Herbert, F. C.; Mallick, S.; Gassensmith, J. J. ZIF-8 Degrades in Cell Media, Serum, and Some-But Not All-Common Laboratory Buffers. *Supramol Chem.* **2019**, *31* (8), 485−490.
(52) Gao, Y.; Zhou, H.; Liu, G.; Wu, J.; Yuan, Y.; Shang, A.; Zhang, Z. G. Tumor Microenvironment: Lactic Acid Promotes Tumor Development. *J. Immunol. Res.* **2022**, *2022*, 3119375.
(53) Lau, N. C.; Lai, Y. C.; Chen, D. W.; Cheng, K. W. Antibacterial Activity Studies of 3D-Printing Polyetheretherketone Substrates with Surface Growth of 2D TiO(2)/ZnO Rodlike Arrays. *ACS Omega* **2022**, *7* (11), 9559−9572.